J Mater Sci (2016) 51:1966–1977
DOI 10.1007/s10853-015-9506-y

Poly(ethylene glycol)-block-poly(propylene glycol)-block-poly (ethylene glycol)-assisted synthesis of graphene/polyaniline composites as high-performance supercapacitor electrodes

Jie Tong[1] · Huaihao Zhang[1] · Jiangna Gu[2] · Lu Li[3] · Chi Ma[1] · Jing Zhao[1] · Chenyin Wang[1]

Received: 23 July 2015 / Accepted: 14 October 2015 / Published online: 19 October 2015

Abstract Graphene/polyaniline (GN/PANI) composites were synthesized by in situ polymerization with the assistance of poly(ethylene glycol)-block-poly(propylene glycol)-block-poly(ethylene glycol) (P123). We show that the addition of P123 enhanced the wettability of GN and hence improved its uniformity in aqueous solution and the dispersity of PANI loaded on GN surface. Structural and morphological analyses indicate that GN has been successfully coated with PANI. P123 was mainly acted as soft temples to improve the control of morphology and increase composites effective specific surface area. Furthermore, it can improve composites capacitive performance as evidenced by electrochemical tests. When the molar ratio of P123 to ANI is 0.0108, the composites exhibit the best performance, in terms of the rate capability, the lowest equivalent series resistance (0.31 Ω) and the charge-transfer resistance (1.46 Ω). Additionally, it achieves a capacity retention of 91.8 % after 1000 charge–discharge cycles at the current density of 500 mA g^{-1}, an increase of 82 % over the composites without P123. A mechanism for interactions of P123, GN, and PANI is proposed in this work.

Electronic supplementary material The online version of this article (doi:10.1007/s10853-015-9506-y) contains supplementary material, which is available to authorized users.

✉ Huaihao Zhang
huaihaozhang@163.com

Jie Tong
tongjie1991@126.com

Jiangna Gu
jiangnagu@163.com

Lu Li
lilu0314@163.com

Chi Ma
chimachi@163.com

Jing Zhao
zhaojing@yzu.edu.cn

Chenyin Wang
wangcy@yzu.cn

[1] College of Chemistry and Chemical Engineering, Yangzhou University, Yangzhou 225002, People's Republic of China

[2] AnKao Energy Co., Ltd, Suzhou 215026, People's Republic of China

[3] HuiCheng (Wuxi) Graphene Technology Application Co. Ltd, Wuxi 214000, People's Republic of China

Introduction

Renewable energies such as wind, solar, and tidal have recently experienced a remarkably rapid growth due to the increasing energy demand [1, 2]. However, the power generated from these sources always fluctuates, thus new energy storage devices are needed to be developed [3]. Supercapacitor has a lot of advantages such as high power density, long cycling life, wide temperature range [4–6]. It can release electric field energy through controlling units when needed, improve stability, and reliability of the system by the instantaneous power compensation. It has wide application prospects in clean power system, aviation, automobile, consumer electronics, and communication areas [4–7].

Currently, the main research of supercapacitor is developing electrode materials characterized by high energy density and steady performance [8–10]. Graphene (GN), a single layer of sp^2-bonded carbon in a honeycomb crystal lattice, is considered to be a kind of new and high efficient

electrode material with high electrical conductivities, specific surface area, and mechanical strength [11, 12]. However, capacitance performance of GN is usually poor as it is prone to conglomeration [13]. Hence, the application of GN alone as electrode material is limited. On the other hand, polyaniline (PANI) is the most outstanding conducting polymer among supercapacitor electrode materials because of its low cost of aniline monomers, better environmental stability, and simple synthesis process [10, 14]. Its unique doping behavior and bulk phase reaction mechanism ensure its good redox reversibility and high pseudocapacitance. Nevertheless, its comparatively low conductivity, low power density, and poor cycling stability limit the application of PANI in supercapacitor [15].

Taking advantage of their energy storage characteristics, combining GN with PANI should be effective to fabricate high-performance electrode materials. Indeed, Wu et al. [16] obtained chemically modified GN/polyaniline nanofibers (PANI-NFs) composite films by vacuum filtration. The film, free-standing and flexible, can be used as working electrode directly. As reported by Zhou et al. [17], GN-wrapped PANI-NFs were prepared by the self-assembly of negatively charged graphene oxide and positively charged PANI-NFs in an aqueous dispersion. Specific capacitance (C_{sp}) of composite electrodes is up to 250 F g^{-1} at the current density of 500 mA g^{-1}. One-step electrochemical synthesis was also used to produce GN/PANI composite films by Feng et al. [18], used in high-performance supercapacitor and H_2O_2 biosensor. Hao et al. [19] fabricated sulfonated GN/PANI nanocomposites by liquid/liquid interfacial polymerization. The C_{sp} of composites is up to 763 F g^{-1} at a scan rate of 1 mV s^{-1}, and its capacity retention is of 96 % after 100 cycles. Currently, main challenges for GN/PANI composites remain to relieve the agglomeration of GN, enhance its surface wettability in aqueous electrolytes, enlarge electrode materials effective specific surface area, and optimize microstructure of PANI.

Surfactants, unique amphiphilic molecules, can be adsorbed on solid surface. Steric hindrance from its long molecular chains can relieve the agglomeration of nanoparticle. Besides, anionic and nonionic surfactants with high surface activities could reduce the surface tension of liquid–liquid and solid–liquid. They can be employed as wetting agents to improve solid surface wettability. In addition, ordered surfactant aggregates, such as micelles, vesicles, and liquid crystals can be acted as micro reactors or soft templates to realize the regulation and control of nanomaterials morphology and structure. In recent years, several researchers have reported the surfactant applied in fabricating supercapacitor electrode materials [20–23]. It is found that surfactants have some influences on morphology, structure, and electrochemical performance of nano-materials.

Triblock copolymer poly(ethylene glycol)-block-poly(propylene glycol)-block-poly(ethylene glycol) (P123), a nonionic surfactant, has been widely used to fabricate ordered mesoporous materials such as SBA-15 [24]. In this paper, we report for the first time that P123 is employed as the assistant agent to prepare GN/PANI composites by one-step in situ polymerization in acid solution. We investigated the influence of P123 addition amount on microstructure and capacitive performance of GN/PANI composites. Analyses by SEM, TEM, low temperature N_2 adsorption, together with electrochemical analysis showed that the composites microstructure and capacitance behavior can be controlled by P123 concentrations. Finally, a mechanism of interaction between P123 and composites was preliminarily proposed.

Experimental

Preparation of GN/PANI composites and working electrodes

Aniline (ANI), ammonium persulfate (APS), hydrochloric acid (HCl) and ethanol (analytically pure) and conductive graphite (chemically reagent) were all obtained from Sinopharm Chemical Reagent Co., Ltd. Pluronic P123 (EO20PO70EO20, average relative molecular weight about 5800) was obtained from Sigma-Aldrich Ltd. GN (Conduction Type-GNSE1231) was supplied by The Sixth Element (Changzhou) Ltd. All raw materials were used directly without further purification. All solutions were prepared using deionized water.

Specific preparation procedures of GN/PANI composites are depicted as follows: Firstly, a certain amount of P123 was added to 20 ml anhydrous ethanol, mechanical stirred until completely dissolved. Secondly, 0.1118 g GN was dispersed into the above solution, stirring for 30 min to get the GN suspension. Thirdly, 20 ml 2 mol dm^{-3} HCl solution dissolved with 0.012 mol ANI was added to the suspension under constantly stirring. Lastly, APS solution (0.004 mol APS dissolved in 40 ml 1 mol dm^{-3} HCl) was added to the above solution to initiate polymerization. The synthesis lasted for 12 h, and GN/PANI composite powder was obtained after filtering, washing, drying, and grinding. Molar ratio of P123 to ANI (n_{P123}/n_{ANI}) was controlled to be 0, 0.0036, 0.0072, 0.0108, 0.0144, and 0.0180. The obtained composites were correspondingly denoted as GP-P0, GP-P1, GP-P2, GP-P3, GP-P4, and GP-P5. Pure PANI was synthesized in the absence of P123 and GN according to above experimental process.

The working electrodes were fabricated by the mixture of 85 wt% active materials, 10 wt% conductive graphite, and 5 wt% polytetrafluoroethylene (PTFE). PTFE was

firstly dispersed in the ethanol under ultrasonic, followed by active materials and graphite. Then, the mixture was grinded adequately to form a paste. The paste was evenly smeared into a foam nickel mesh (1×1 cm^2) and then dried in a vacuum oven at 60 °C for 8 h. Lastly, the electrode was pressed into a thin sheet under the pressure of 10 MPa to ensure a good electrical contact between active materials and foam nickel mesh.

Material characterization

Structure of GN/PANI composites was analyzed by X-ray diffraction (XRD), Fourier transform infrared spectroscopy (FTIR), X-ray photoelectron spectroscopy (XPS), and low temperature N_2 adsorption. Thereinto, XRD, recorded from 10° to 80° (2θ angle), was carried out with Cu Kα radiation ($\lambda = 0.15406$ nm) on a Bruker D8 super speed X-ray diffractometer. FTIR spectra were recorded by a Bruker Tensor 27 spectrometer with KBr pellets from 4000 to 400 cm^{-1}. XPS was performed on ESCALAB250Xi Photoelectron Spectrometer (ThermoFisher Scientific Ltd.) with Al Kα radiation as the excitation source. Low temperature N_2 adsorption was conducted by automatic analyzers TriStar 3000 to characterize samples pore texture properties. Morphology of composites was observed by S-4800 II field emission scanning electron microscope (FESEM, 20 kV) and Philips TECNAI 12 transmission electron microscope (TEM) (Hitachi Ltd., Japan).

Electrochemical measurements

All electrochemical measurements were performed in 1 mol dm^{-3} KNO_3 aqueous electrolyte by a three-electrode system (samples as the working electrode, activated carbon as the counter electrode, and saturated calomel electrode (SCE) as the reference electrode) at room temperature. Cyclic Voltammetry (CV) and Galvanostatic Charge–Discharge (GCD) tests were conducted by CHI660E electrochemical workstation (Chenghua, Shanghai China) within a potential range of −0.4 to 0.4 V. Scan rates and current densities were set from 5 to 100 mV s^{-1} and 500 to 5000 mA g^{-1}, respectively. Electrochemical impedance spectroscopy (EIS) tests, with alternating current signal amplitude set at 5 mV, were carried out on AutoLab-PGSTAT30 (Netherlands) within the frequency range of 10^{-2} to 10^5 Hz.

Results and discussion

Structure and morphology characterizations

Figure 1a shows XRD patterns of samples. For PANI, crystalline peaks at $2\theta = 15.3°$, 25.3° and 20.2°, caused by periodicity perpendicular, parallel to the polymer chain and layers of polymer chains of alternating distance, respectively, can be attributed to (011), (200) and (020) crystal planes of conductive PANI-NFs [25–27]. Diffraction peaks of GN appear at $2\theta = 25.9°$ and 42.6° correspond to the graphite-like structure (002) and (100) crystal planes, respectively [28]. Peaks of all composites are very similar likely the superimposed of PANI and GN, indicating that P123 has no effect on GN/PANI composites crystal structure, and GN and PANI has been combined successfully. Nevertheless, GN diffraction peak at $2\theta = 42.6°$ is weaker, suggesting GN surface has been widely coated by PANI nanoparticles. FTIR spectra of samples are shown in Fig. 1b. Spectrum of GN is basically a straight line without characteristic bands, demonstrating that GN is a perfectly reduced state [29]. For PANI, several bands can be observed in its spectrum, suggesting the generation of doped PANI in its emeraldine salt (ES) form [17]. Characteristic bands of GP-P0 and GP-P3 are all similar to that of PANI, indicating the negligible effect of P123 on composites structure. Moreover, no characteristic band of P123 is observed in spectra of composites, implying that most surface P123 has been removed by washing process.

The wide scan XPS spectrum (Fig. 2) indicates that GP-P3 is mainly composed of C, N, and O elements. In general, content of element can be calculated by peak area. Specifically, C/N ratio of GP-P3 surface is 7.3:1 while theoretical value of pure PANI is 6:1, implying that most of GN surface has been covered with PANI. Extra C may come from GN not covered by PANI. Exposed GN surface may be ascribed to the interaction between PANI particles. In addition, appearance of O may be attributed to H_2O, residual P123 in composites or residual carboxylic groups of GN. C1 s spectrum can be deconvoluted into four Gaussian peaks, corresponding to C–C/C=C (284.8 eV), C-N (285.5 eV), C–O–C (286.4 eV), and C=O/O=O–O (290.0 eV), respectively [30, 31]. The presence of ether and carbonyl groups further confirms the existence of P123 and oxygen-containing groups of GN surface. Certainly, quantity of these impurities is little. On the other hand, N1 s spectrum can be decomposed into three different peaks, with binding energies at 400.0 (C=N–C), 400.5 (C-NH-C), and 404.7 eV (C-N^+-C), respectively [31]. Thereinto, the existence of –N^+– suggests the formation of doped PANI. XPS analysis is basically consistent with XRD and FTIR.

In Fig. 3a, brightness of GN sheets is uneven despite its good transparency, implying that parts of them are multilayer and congregated together. Its agglomeration is very obvious in Fig. 4a. Pure PANI obtained in this work are all stumpy PANI-NFs, interweaved into a low voidage complex network (see Figs. 3b, 4b). If such PANI and GN with serious agglomeration are used as electrode material alone,

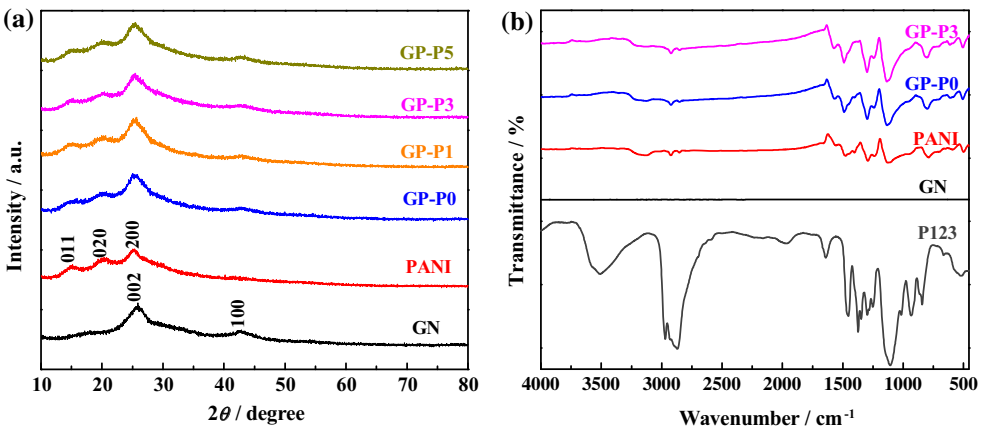

Fig. 1 **a** XRD patterns and **b** FTIR spectra of samples

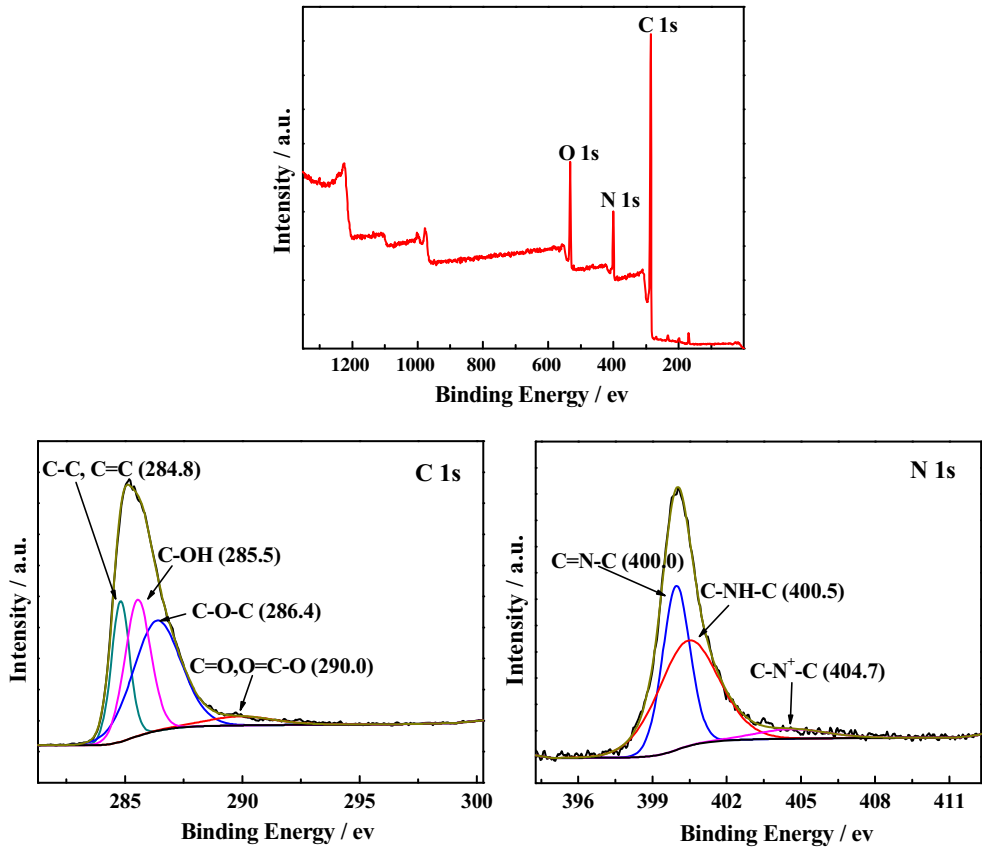

Fig. 2 XPS spectrum of GP-P3 and core levels of C 1 s, N 1 s

the intercalation/de-intercalation of electrolyte ions can only be performed on the limited network surface. As a result, its utilization ratio and capacitance performance would be poor.

In Fig. 3, brightness of GN sheets is weaker than that of GN/PANI composites, indicating PANI has widely loaded on GN surface. According to previous studies [32], oxidative polymerization of PANI contains two competitive processes: homogeneous nucleation in bulk solution and heterogeneous nucleation on GN sheet. The latter can be performed preferentially with the presence of GN. The lower right of Fig. 4e is the magnification of part 1, herein, a large amount of oligomer spherical PANI (OS-PANI) can be seen on GN surface. OS-PANI coated GN structure (OS-PANI/GN) is more obvious in Fig. S1. The lower left of Fig. 4e is the magnification of part 2, showing a relatively homogenously distribution of PANI-NFs on the surface of OS-PANI/GN. OS-PANI and PANI-NFs might be

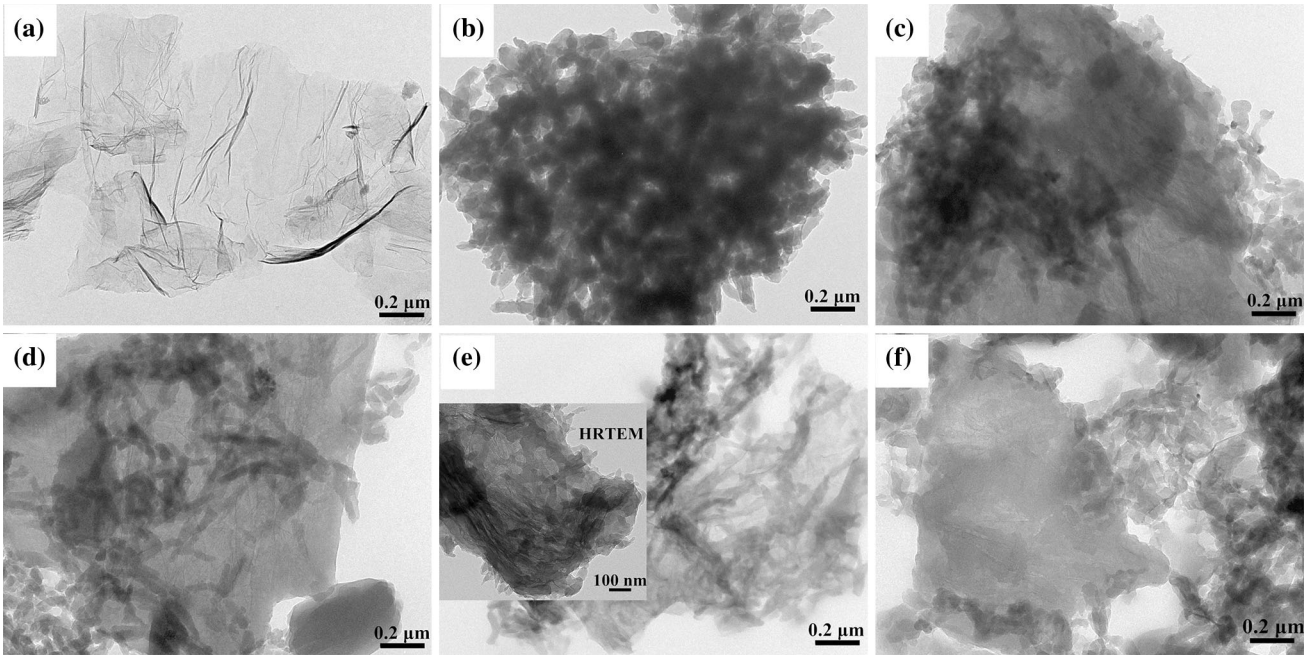

Fig. 3 TEM images of GN (**a**), PANI (**b**), GP-P0 (**c**), GP-P1 (**d**), GP-P3 (**e**), GP-P5 (**f**)

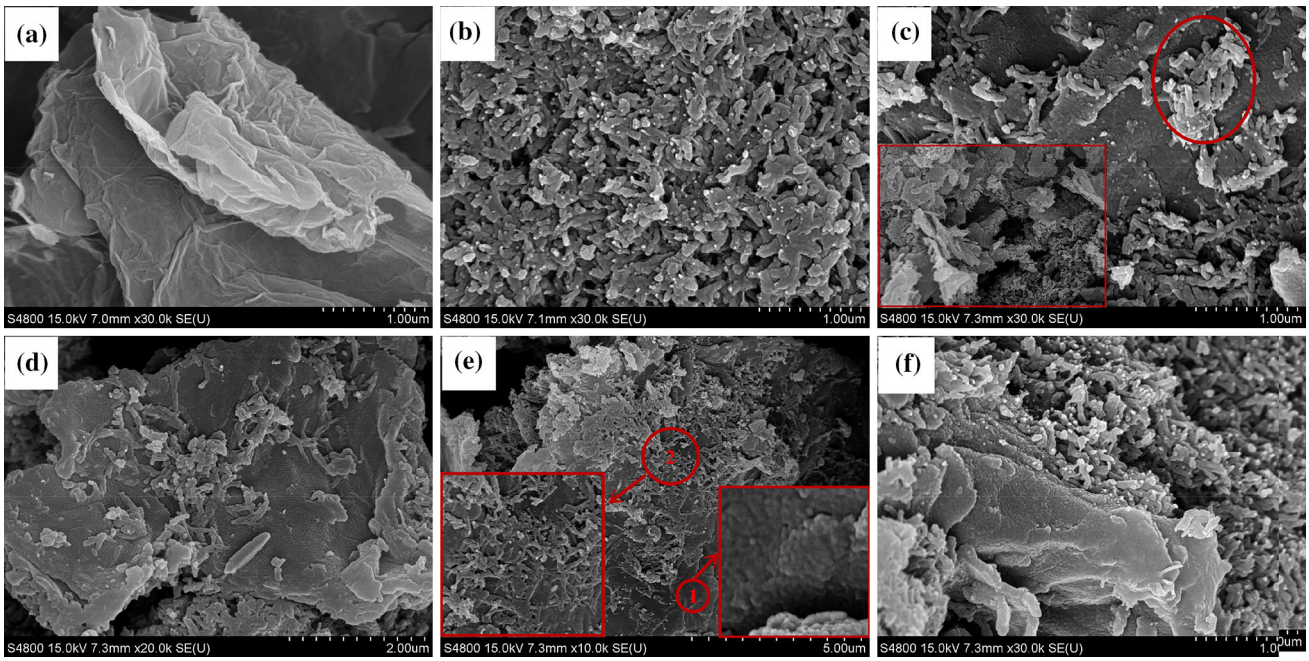

Fig. 4 SEM images of GN (**a**), PANI (**b**), GP-P0 (**c**), GP-P1 (**d**), GP-P3 (**e**), GP-P5 (**f**)

produced from heterogeneous nucleation and homogeneous nucleation, respectively. Structure of GN/PANI composites are basically the same as the sandwich structure of GP-P3, and the main difference is the distribution of PANI-NFs. Inset in Fig. 4c is the SEM image of GP-P0 at low magnification. PANI-NFs and GN are severely agglomerated. The inter-mixing degree of two individual components is low. The reason may be GN layers fold together without P123 and hence its surface utilization is low. In other words, the effective contact area between ANI monomers and GN surface is small, and most PANIs are generated from homogeneous nucleation. With the increase of P123

addition amount, shown in Figs. 3c–e and 4c–e, dispersity of PANI-NFs on OS-PANI/GN surface was improved. Inset of Fig. 3e is the HRTEM image. Obviously, distribution of PANI-NFs in GP-P3 is the most uniform and the inter-mixing degree of two single components is the highest, ascribing to the steric hindrance effect of macromolecule P123. However, excessive P123 will result in relatively low degree of compound mixing. Indeed, when the molar ratio of P123 to ANI is 0.018 (Figs. 3f and 4f), large amounts of PANI-NFs grow outward along the edge of OS-PANI/GN composites. It might be attributed to that P123 self-assembling into spherical or rod-like micelles with enormous size, absorbing on the surface of OS-PANI/GN. Electrostatic repulsion and steric hindrance of P123 force these PANI-NFs to generate only along OS-PANI/GN composites edge. P123 in this work acted as soft templates to control the morphology of GN/PANI composites, rather participated the chemical synthesis of composites. It can be further confirmed by the weight ratios of PANI to GN listed in Table S1. Weight ratios are basically the same though the composites were obtained with the assistance of different amounts P123.

Based on the data of D in Table 1, all samples can be considered as mesoporous materials (2-50 nm), conducive to electrochemical energy storage. Structure parameters of GN/PANI composites, especially S_{BET} and S_{Meso}, are lower than those of GN but closer to those of pure PANI, indicating that GN surface has been coated by a layer of dense PANI. It coincides well with SEM and TEM results. Furthermore, by comparing the textural properties of samples prepared with/without the assistance of P123, P123 is favorable in improving GN/PANI composites textural properties in general. With the increase of P123 addition amount, all parameters increase at first and then decrease. GP-P3 having the highest specific surface area, largest pore volume, and best average pore size, conducive to the intercalation/deintercalation of electrolyte ions and the improvement of electrodes capacitance performance. Therefore, 0.0108 can be ensured as the optimal molar ration of P123 to ANI in the preparation of GN/PANI composites.

Capacitance behavior

In Fig. 5a, CV curves of GN are approximately rectangular, implying an ideal electric double-layer behavior [19]. A remarkable growth of current density response is observed with the increase of scan rates, demonstrating the excellent rate capability of GN [33]. For PANI (Fig. 5b), redox peaks can be attributed to the redox process of PANI between its leucoemeraldine form and polaronic emeraldine forms [25, 34]. With the increase of scan rates, the increase range of enclosed curves areas decreases, suggesting poor rate performance of PANI. Several more obvious redox peaks appear in Fig. 5c, indicating pseudocapacitive performance of PANI among GP-P3 is better than pure PANI with low voidage network structure. Hereinto, morphology of PANI is modified by P123. With the increase of scan rates, the current response of GP-P3 increases clearly, implying good rate properties. In addition, an anodic shift of oxidation peaks and a cathodic shift of reduction peaks on GP-P3 CV curves are due to the resistance of electrode [35]. In general, the larger the enclosed CV curves areas, the greater the C_{sp}. From Fig. 5d, enclosed areas of GN/PANI composites are all greater than that of pure PANI, increasing at first and then decreasing with the increase of P123. GP-P3 obtains the largest enclosed areas, suggesting the highest C_{sp}. It can be explained that surface utilization of GN is the highest and morphology of PANI loaded on GN surface is the most regular with the optimal P123 ($n_{P123}/n_{ANI} = 0.0108$). GP-P3 is most porous and it has the largest specific surface area. Consequently, static capacitance of GN and pseudocapacitance of PANI can be fully exploited to improve C_{sp} and rate capability of GN/PANI composites.

In Fig. 6a, the deviation from linearity for curves of GN/PANI composites is due to the existence of pseudocapacitance [36], implying that capacitances of PANI and composites are mainly derived from pseudocapacitive behavior. The deviation degree of GP-P1, 2, 3, 4, and 5 are basically the same and are all lower than that of pure PANI and GP-P0 (Table S2), indicating the double-layer

Table 1 Textural properties of Samples

Samples	S_{BET} ($m^2\ g^{-1}$)	S_{Meso} ($m^2\ g^{-1}$)	V_{Meso} ($cm^3\ g^{-1}$)	V_{Total} ($cm^3\ g^{-1}$)	D (nm)
GN	78.0	127.1	0.26	0.31	15.8
PANI	35.4	28.6	0.17	0.23	26.2
GP-P0	32.8	23.7	0.10	0.14	17.3
GP-P1	34.5	29.3	0.12	0.17	19.3
GP-P3	37.6	33.0	0.15	0.19	20.4
GP-P5	36.8	28.6	0.12	0.18	19.6

S_{BET} BET, (Brunauer–Emmett–Teller) surface area; S_{Meso} and V_{Meso}, The mesoporous surface area and mesoporous volume, calculated from the t-plot method; V_{Total}, Total pore volume, measured at $P/P_0 = 0.99$; D, Average pore size, calculated by $4V_{Total}/S_{BET}$

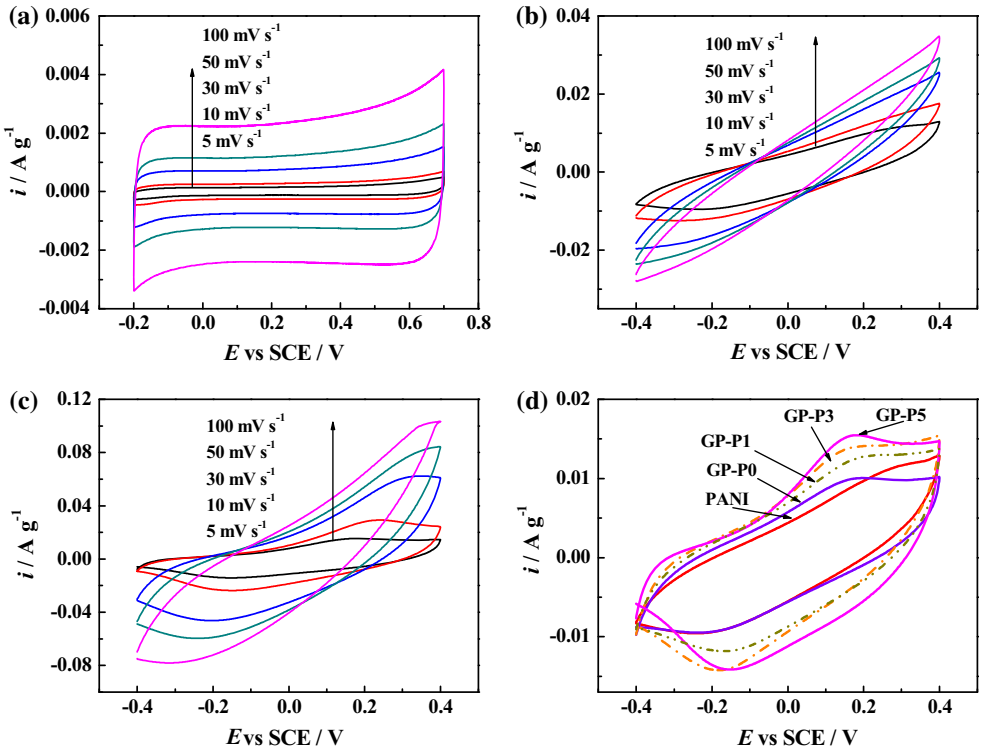

Fig. 5 CV curves of GN (**a**), PANI (**b**), GP-P3 (**c**) electrodes at different scan rates; of PANI and GN/PANI composites at 5 mv s^{-1} in 1 mol dm^{-3} KNO_3 (**d**)

capacitance performance of P123-assisted composites is more remarkable, or rather, specific surface area of these samples is larger. GCD curves of samples produced with P123 are all more symmetric than those of pure PANI and GP-P0, indicating a better reversibility of charge–discharge reaction and a lower resistance of such samples [37]. Symmetry of GP-P3 curve is the best. By comparing discharge curves in Fig. 6b, P123 undoubtedly prolongs the discharge duration of electrodes. Moreover, with the increase of P123, the discharge time increases initially and then decreases. GP-P3 obtains the largest discharge time, or the largest C_{sp}, which is consistent with the conclusion from CV curves. Within the potential window of −0.4 to −0.2 V, the discharge magnitude of composites decreased and the resistance increased, ascribing to the increasing conductivity from the continuous undoping process of PANI [36].

C_{sp} of PANI and a series of GN/PANI composites at different current densities are calculated according to the following equation:

$$C_{sp} = I \times \Delta t/(m \times \Delta V), \quad (1)$$

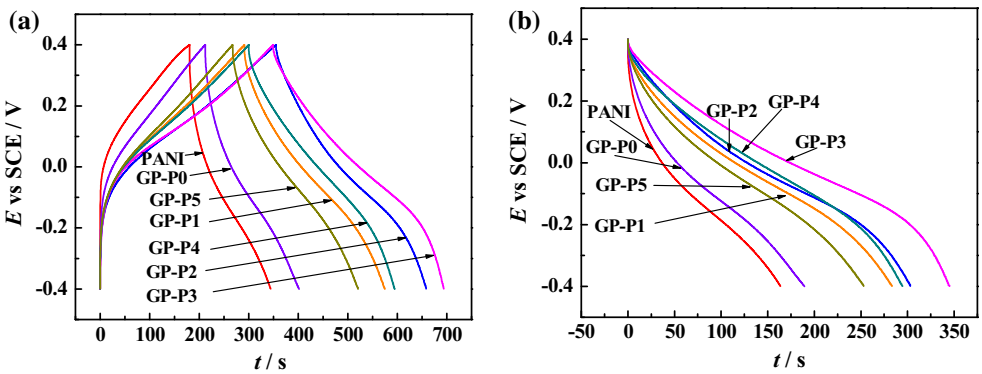

Fig. 6 GCD curves (**a**) and discharge curves (**b**) of electrodes at a current density of 500 mA g^{-1}

where I is the charge–discharge current (A), Δt is the discharge time (s), m is the active material mass of working electrode (g), ΔV is the potential difference during discharge process (V), and C_{sp} is the electrode specific capacitance (F g^{-1}). Specific data are shown in Table 2. Due to the agglomeration of GN, a low C_{sp} value 10.2 F g^{-1} is obtained at a current density of 500 mA g^{-1}, while PANI and GP-P0 are, respectively, 102.3 and 118.5 F g^{-1}. C_{sp} of GP-P0 is larger than the sum of those of GN and PANI. This could be due to the synergistic effect of GN and PANI. That is, on the one hand, GN can provide PANI with an ideal conductive network, enhancing the degree of Faradaic reaction between the PANI and the electrolyte; on the other hand, PANI coated on GN surface can prevent the re-aggregation of GN sheets. Synergistic effect of GN and PANI is undoubtedly conducive to improve single component utilization ratio and hence to increase capacitance of composites. From the comparison of GP-P0- and P123-assisted composites, the addition of P123 significantly increased composites C_{sp} values, confirming the positive effect of P123 on improving composites capacitance performance. With the continued increase of P123 addition amount, C_{sp} value of composite materials first increases, reaching a maximal value of 215.8 F g^{-1} for GP-P3, before decreases. All C_{sp} values in Table 2 decrease with the increase of the current density. This is because electrolyte ions do not have enough time to diffuse into deep pores of active materials at high current density, thus the insertion/de-insertion is limited on the surface or in shallow pores of electrode materials, resulting in the decrease of the utilization efficiency of composites [38]. As for rate capability, PANI is poor due to its pseudocapacitive behavior. GP-P0 with GN is slightly superior to PANI. For GP-P3, a high C_{sp} 157.2 F g^{-1} is maintained at a current density of 5000 mA g^{-1}, ascribing to the abundant pores suitable for electrolyte ions fast-moving (as shown in Table 1).

Figure 7a shows the SEM image of GP-P3 electrode before 1000 charge–discharge cycles. Because of the pressure of 10 MPa, the electrode surface is very flat. Materials on the surface should be PANI. After 1000 cycles, many cracks appeared at the surface (Fig. 7b). Two reasons could be account for this phenomenon: (1) the structure of the electrode is too dense, the continuous movement of electrolyte ions is easy to breakdown its surface; (2) the continuous swelling and shrinkage of PANI during the charge/discharge process resulted in a fragmentation of macromolecule chain. Appearance of cracks may lead to a decrease of capacitance. In Fig. 7c, a C_{sp} value of 61.4 F g^{-1} is retained after 1000 charge–discharge cycles of PANI, with only 59.9 % capacity retained. Comparatively, GP-P0 exhibits a better cycling life with the capacity retention of 89.2 %. It can be ascribed to the synergistic effect of GN for inhibiting the structural failure of PANI. At a current density of 500 mA g^{-1}, C_{sp} value of GP-P3 is up to 215.8 F g^{-1} and its capacitance after 1000 charge–discharge cycles retains 91.8 %, increased by 82 and 2.9 % individually in comparison with GP-P0, suggesting P123 has a positive effect on improving composites cycle performance. Capacity retention of GP-P3 is higher than those reported values [16–18].

In Fig. 7d, the x intercept of Nyquist plots corresponds to equivalent series resistance (R_s), including intrinsic resistance of active material, electrolyte resistance, and contact resistance between electrolyte and electrode [33, 38]. According to Table 3, R_s of GN/PANI composites are all slightly lower than that of PANI (0.38 Ω), indicating that the synergistic effect between GN and PANI is helpful to reduce R_s. Thereinto, R_s of GP-P3 is the smallest. In high frequency region of Nyquist plots, diameter of the semicircle represents ionic charge-transfer resistance (R_{ct}) of the layer on the electrode [39]. In general, the larger the diameter is, the higher the R_{ct} will be and the poorer the conductivity is. From the inset in Fig. 7d, all semicircle diameters of composites are smaller than that of pure PANI, suggesting both GN and P123 are all conductive to decrease R_{ct} and improve composites conductivity. Meanwhile, GP-P3 obtains a smallest R_{ct} of 1.46 Ω (Table 3). In intermediate frequency area, electrodes reaction process is controlled by diffusion procedure [21]. Nyquist plots in this part evolve into an oblique line with the slope equal to 1.

Table 2 Specific capacitances of PANI and a series of GN/PANI composites at different current densities in 1 mol dm^{-3} KNO_3

C_{sp}/F g^{-1}									
Sample		GN	PANI	GP-P0	GP-P1	GP-P2	GP-P3	GP-P4	GP-P5
i/mA g^{-1}	500	10.2	102.3	118.5	177.2	192. 5	215.8	184.2	158.2
	800	–	58.7	86.9	152.0	185.4	205.8	164.8	130.1
	1000	9.7	45.2	71.6	143. 5	185.0	201.5	158.9	113.9
	1500	–	21.8	55.1	124.7	172.4	183.8	140.1	97.2
	2000	9.4	9.8	44.1	95.6	158.9	168.7	113.7	82.6
	5000	9.3	1.9	30.2	74.9	138.6	157.2	91.6	63.1

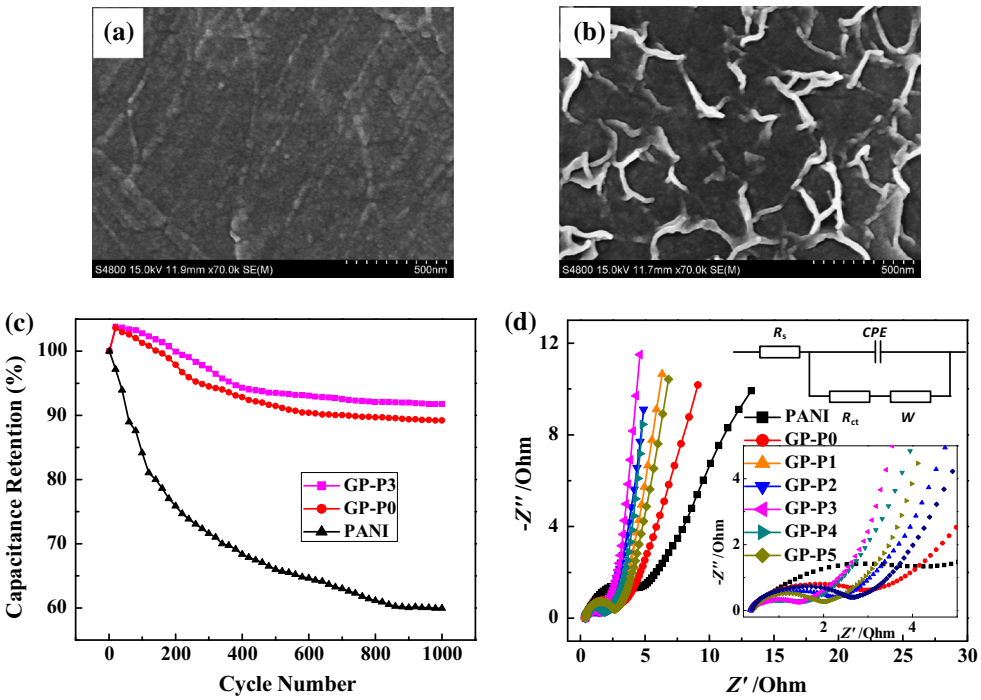

Fig. 7 SEM images of GP-P3 pasted on Ni foam before (**a**) and after (**b**) 1000 cycles; **c** 1000 charge–discharge cycles stability curves of electrodes at a current density of 500 mA g^{-1}; **d** Nyquist plots of electrodes. Inset is the amplified image of Nyquist plots in high frequency region and circuit diagram equivalent

Table 3 Equivalent circuit diagram parameters of samples

Samples	PANI	GP-P0	GP-P1	GP-P2	GP-P3	GP-P4	GP-P5
R_s/Ω	0.38	0.34	0.33	0.32	0.31	0.34	0.36
R_{ct}/Ω	4.48	2.05	1.64	1.52	1.46	1.55	1.99
W/Ω	0.74	4.6	3.66	3.37	3.16	3.33	3.38
CPE/mF	15.82	2.56	3.69	3.68	3.7	2.49	1.82

The more the slopes are closer to 1, the easier for the conduction of the diffusion process. Resistance in this part is named as Warburg impedance (*W*). Mesoporous structure and large pore size of electrode materials are favorable to decrease *W* [40]. According to previous analysis, GP-P3 possesses the most abundant mesoporous and the largest pore size compared to other composites. Therefore, *W* of GP-P3 should be the minimum, well consistent with Nyquist plots. However, in Table 3, *W* of GN/PANI composites are all larger than that of pure PANI, which could be related to the variety of PANI forms in composites [41]. At the low frequency part, there is a nearly vertical line. The more vertical the line is, the more ideal the capacitor for the supercapacitor will be [39]. Obviously, the deviation rate between pure PANI curve and vertical line is the largest, suggesting the assistance of P123 is helpful to optimize the capacitance behavior of GN/PANI composites. Curve of GP-P3 is the most vertical, indicating 0.0108 is the optimal molar ratio of P123 to ANI. In general, the higher the constant phase element (*CPE*) values, the quicker is the formation of electric double layer [42]. Thereinto, GP-P3 owns the maximum *CPE* among composites as is shown in Table 3.

Function mechanism of P123

Figure 8 illustrates possible procedures of the generation of GN/PANI composites with P123. Accordingly, amphipathic macromolecule P123 is firstly adsorbed by electrostatic interaction on the surface of GN sheet to enhance its surface wettability and hence to improve its dispersity and uniformity in aqueous solution (Fig. 8a) [43]. Secondly, due to the steric hindrance of macromolecule P123, some surfaces of GN are unoccupied. Owing to the electrostatic force, positively charged ANI monomers are absorbed on negatively charged GN surface (Fig. 8b) [17]. Nucleation sites distributed heterogeneously on GN surface nucleate and generate OS-PANI at the beginning of polymerization [32]. Meanwhile, P123 is competitively displaced by OS-PANI particle, because the interactions of π-π conjugation, hydrogen bonding, and electrostatic force between GN and PANI [17] are larger than intermolecular forces between GN and P123. With polymerization reaction carried through, the initial PANI coated GN structure can be produced (Fig. 8c). Finally, homogeneous nucleation plays the leading role in polymerization [32], nucleation points are redistributed again on PANI surface. ANI monomers are

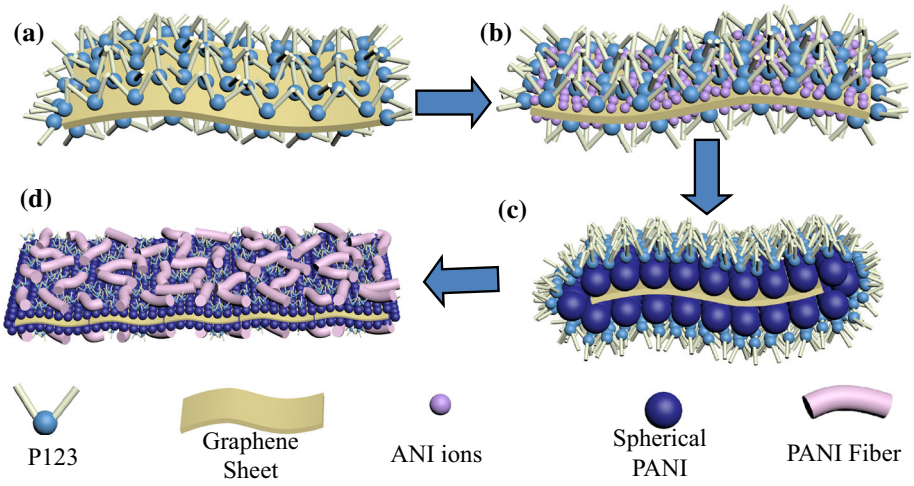

Fig. 8 Illustration of possible procedures of the generation of GN/PANI composites with the assistance of P123

polymerized to PANI-NFs along the surface of PANI spherical particle. Due to the steric hindrance of P123, distribution of PANI-NFs is uniform (Fig. 8d). When the addition amount of P123 is optimal ($n_{P123}/n_{ANI} = 0.0108$), the structure of GN/PANI composites will be almost the same to Fig. 8d. Consequently, the utilization ratio of GN and PANI, as well as capacitive performance of composite materials can be improved.

Conclusions

GN/PANI composites were fabricated by one-step in situ polymerization in acid solution with the assistance of P123. According to FTIR and XRD tests, P123 on materials surface has been mostly removed by washing process and has little effect on GN/PANI composites crystal structure. XPS spectra indicate that GN surface has been covered with PANI. SEM and TEM demonstrate that PANI-NFs are loaded on OS-PANI/GN surface, indicating P123 indeed has impacted the morphology of GN/PANI composites. In particular, dispersity of PANI-NFs as well as the degree of the mixing between GN and PANI is the most optimal when $n_{P123}/n_{ANI} = 0.0108$. N_2 physical adsorption data prove that GP-P3 possesses the highest specific surface area 37.6 $m^2\ g^{-1}$, pore volume 0.19 $cm^3\ g^{-1}$ and average pore size 20.4 nm among all composites. The same mass ratio of single components in GN/PANI composites and above characterizations suggested that P123 in this work major functioned as soft templates to control the composites morphology. Specifically, P123 could promote PANI to well-grown and well-dispersed on GN surface, enhancing the effective utilization of two single components. In addition, P123 ensured PANI with abundant pores, enabling a fast Faradaic reaction and providing a short ion diffusion path during the charge–discharge process. Combined with electrochemical tests, it can be confirmed that P123 is helpful to improve capacitive performance of GN/PANI composites. Comprehensive properties of GP-P3 are the best. In detail, specific capacitance of GP-P3 is up to 215.8 F g^{-1} at the current density of 500 mA g^{-1}, increased by 82 % in comparison with GP-P0. Its capacity retention after 1000 charge–discharge cycles is 91.8 and 2.9 % higher than that of GP-P0. Additionally, equivalent series resistance (R_s), charge-transfer resistance (R_{ct}), and Warburg impedance of GP-P3 are the smallest among all composites. Applying P123 to the fabrication of GN/PANI composite electrodes is an effective way.

Acknowledgements This work was financially supported by the Natural Science Foundation of China (Nos. 21106124 and 21375116) and Postdoctoral Science Foundation of China (2014M551668). The related measure and analysis instrument for this work was supported by the Testing Center of Yangzhou University.

References

1. Chen JC, Liu YQ, Li WJ, Wu C, Xu LQ, Yang H (2015) Nanostructured polystyrene/polyaniline/graphene hybrid materials for electrochemical supercapacitor and Na-ion battery applications. J Mater Sci 50:5466–5474. doi:10.1007/s10853-015-9092-z
2. Thounthong P, Chunkag V, Sethakul P, Sikkabut S, Pierfederici S, Davat B (2011) Energy management of fuel cell/solar cell/supercapacitor hybrid power source. J Power Sources 196:313–324
3. Kinjo T, Senjyu T, Urasaki N, Fujita H (2006) Output levelling of renewable energy by electric double-layer capacitor applied for energy storage system. IEEE Trans Energy Convers 21:221–227
4. Zhu T, Zheng SJ, Chen YG, Luo J, Guo HB, Chen YE (2014) Improvement of hydrothermally synthesized MnO_2 electrodes on Ni foams via facile annealing for supercapacitor applications. J Mater Sci 49:6118–6126. doi:10.1007/s10853-014-8343-8

5. Vidhyadharan B, Zain NKM, Misnon II, Aziz RA, Ismail J, Yusoff MM, Jose R (2014) High performance supercapacitor electrodes from electrospun nickel oxide nanowires. J Alloys Compd 610:143–150
6. Fu Y, Song JM, Zhu YQ, Cao CB (2014) High-performance supercapacitor electrode based on amorphous mesoporous $Ni(OH)_2$ nanoboxes. J Power Sources 262:344–348
7. Abdelkafi A, Krichen L (2014) Energy management optimization of a hybrid power production unit based renewable energies. Int J Electr Power Energy Syst 62:1–9
8. Cao F, Pan GX, Xia XH, Tang PS, Chen HF (2014) Synthesis of hierarchical porous NiO nanotube arrays for supercapacitor application. J Power Sources 264:161–167
9. Sarangapani S, Tilak BV, Chen CP (1996) Materials for electrochemical capacitors theoretical and experimental constraints. J Electrochem Soc 143:3791–3799
10. Xiong P, Hu CY, Fan Y, Zhang WY, Zhu JW, Wang X (2014) Ternary manganese ferrite/graphene/polyaniline nanostructure with enhanced electrochemical capacitance performance. J Power Sour 266:384–392
11. Geim AK (2009) Graphene: status and prospects. Science 324:1530–1534
12. Chen AB, Yu YF, Xing TT, Wang RJ, Zhang Y, Li Q (2015) Synthesis of graphitic carbon spheres for enhanced supercapacitor performance. J Mater Sci 50:5578–5582. doi:10.1007/s10853-015-9106-x
13. Jiang ZJ, Jiang ZQ, Chen WH (2014) The role of holes in improving the performance of nitrogen-doped holey graphene as an active electrode material for supercapacitor and oxygen reduction reaction. J Power Sources 251:55–65
14. Wang DW, Li F, Zhao JP, Ren W, Chen ZG, Tan J, Wu ZS, Gentle L, Lu GQ, Cheng HM (2009) Fabrication of graphene/polyaniline composite paper via in situ anodic electropolymerization for high-performance flexible electrode. ACS Nano 3:1745–1752
15. Cong HP, Ren XC, Wang P, Yu SH (2013) Flexible graphene-polyaniline composite paper for high-performance supercapacitor. Energy Environ Sci 6:1185–1191
16. Wu Q, Xu YX, Yao ZY, Liu AR, Shi GQ (2010) Supercapacitors based on flexible graphene/polyaniline nanofiber composite films. ACS Nano 4:1963–1970
17. Zhou SP, Zhang HM, Zhao Q, Wang XH, Li J, Wang FS (2013) Graphene-wrapped polyaniline nanofibers as electrode materials for organic supercapacitors. Carbon 52:440–450
18. Feng XM, Li RM, Ma YW, Chen RF, Shi NE, Fan QL, Huang W (2011) One-Step electrochemical synthesis of graphene/polyaniline composite film and its applications. Adv Funct Mater 21:2989–2996
19. Hao QL, Wang HL, Yang XJ, Lu LD, Wang X (2011) Morphology-controlled fabrication of sulfonated graphene/polyaniline nanocomposites by liquid/liquid interfacial polymerization and investigation of their electrochemical properties. Nano Res 4:323–333
20. Zhao T, Jiang H, Ma J (2011) Surfactant-assisted electrochemical deposition of α-cobalt hydroxide for supercapacitors. J Power Sour 196:860–864
21. Singu BS, Male U, Srinivasan P, Pabba S (2014) Use of surfactant in aniline polymerization with TiO_2 to PANI-TiO_2 for supercapacitor performance. J Solid State Electrochem 18:1995–2003
22. Jiang RR, Huang T, Liu JL, Zhuang JH, Yu AS (2009) A novel method to prepare nanostructured manganese dioxide and its electrochemical properties as a supercapacitor electrode. Electrochim Acta 54:3047–3052
23. Zhang HH, Wang YQ, Liu CW (2012) Influence of surfactant CTAB on the electrochemical performance of manganese dioxide used as supercapacitor electrode material. J Alloys Compd 517:1–8
24. Roux EL, Liang Y, Törnroos KW, Nief F, Anwander R (2012) Heterogenization of lanthanum and neodymium monophosphacyclopentadienyl bis(tetramethylaluminate) complexes onto periodic mesoporous silica SBA-15. Organometallics 31:6526–6537
25. Li YZ, Zhao X, Xu Q, Zhang QH, Chen DJ (2011) Facile preparation and enhanced capacitance of the polyaniline/sodium alginate nanofiber network for supercapacitors. Langmuir 27:6458–6463
26. Li YZ, Zhang QH, Zhao X, Yu PP, Wu LH, Chen DJ (2012) Enhanced electrochemical performance of polyaniline/sulfonated polyhedral oligosilsesquioxane nanocomposites with porous and ordered hierarchical nanostructure. J Mater Chem 22:1884–1892
27. Yan J, Wei T, Shao B, Fan ZJ, Qian WZ, Zhang ML, Wei F (2010) Preparation of a graphene nanosheet/polyaniline composite with high specific capacitance. Carbon 48:487–493
28. Kuilla T, Bhadra S, Yao D, Kimc NH, Bosed S, Lee JH (2010) Recent advances in graphene based polymer composites. Prog Polym Sci 35:1350–1375
29. Bose S, Kuila T, Mishra AK, Kim Lee JH (2012) Dual role of glycine as a chemical functionalizer and a reducing agent in the preparation of graphene: an environmentally friendly method. J Mater Chem 22:9696–9703
30. Shin HJ, Kim KK, Benayad A, Yoon SM, Park HK, Jung IS, Jin MH, Jeong HK, Kim JM, Choi JY, Lee YH (2009) Efficient reduction of graphite oxide by sodium borohydride and its effect on electrical conductance. Adv Energy Mater 19:1987–1992
31. Liu Y, Wang HH, Zhou J, Bian LY, Zhu EW, Hai JF, Tang J, Tang WH (2013) Graphene/polypyrrole intercalating nanocomposites as supercapacitors electrode. Electrochim Acta 112:44–52
32. Xu JJ, Wang K, Zu SZ, Han BH, Wei ZX (2010) Hierarchical nanocomposites of polyaniline nanowire arrays on graphene oxide sheets with synergistic effect for energy storage. ACS Nano 4:5019–5026
33. Zhang HH, Gu JN, Jiang YY, Wang YQ, Zhao J, Zhang XX, Wang CY (2014) Calcination removing soft template cetyl trimethyl ammonium bromide and its effects on capacitance performance of supercapacitor electrode MnO_2. Energy Convers Manag 86:605–613
34. Xu YF, Schwab MG, Strudwick AJ, Hennig I, Feng XL, Wu ZS, Müllen K (2013) Screen-printable thin film supercapacitor device utilizing graphene/polyaniline inks. Adv Energy Mater 3:1035–1040
35. Zhang K, Mao L, Zhang LL, Chan HSO, Zhao XS, Wu JS (2011) Surfactant-intercalated, chemically reduced graphene oxide for high performance supercapacitor electrodes. J Mater Chem 21:7302–7307
36. Mao L, Zhang K, Chan HSO, Wu JS (2012) Surfactant-stabilized graphene/polyaniline nanofiber composites for high performance supercapacitor electrode. 22:80–85
37. Wang MR, Zhang HH, Wang CY, Hu XY, Wang GX (2013) Direct electrosynthesis of poly-o-phenylenediamine bulk materials for supercapacitor application. Electrochim Acta 91:144–151
38. Zhang HH, Gu JN, Tong J, Ma C, Zhao J, Zhang XX, Wang CY (2015) Poly(ethylene oxide)–poly(propylene oxide)–poly(ethyl oxide) enhancing capacitance behavior of composite electrode material poly(o-phenylenediamine)/manganese dioxide for supercapacitor. Energy Convers Manag 91:120–131
39. Wang Y, Shi ZQ, Huang Y, Ma YF, Wang CY, Chen MM, Chen YS (2009) Supercapacitor devices based on graphene materials. J Phys Chem C 113:13103–13107
40. Zhou J, Li W, Xing W, Zhou SP (2011) Capacitive performance of tunable ordered mesoporous carbons in organic and H_2SO_4 electrolyte. Acta Phys-Chim Sin 27:1431–1438

41. Hu CC, Chu CH (2001) Electrochemical impedance characterization of polyaniline-coated graphite electrodes for electrochemical capacitors-effects of film coverage/thickness and anions. J Electroanal Chem 503:105–116
42. Osório WR, Peixoto LC, Garcia A (2009) The effects of Ag content and dendrite spacing on the electrochemical behavior of PbeAg alloys for Pb-acid battery components. Int J Electrochem Sci 4:820–831
43. Kong LB, Zhang J, An JJ, Luo YC, Kang L (2008) MWNTs/PANI composite materials prepared by in situ chemical oxidative polymerization for supercapacitor electrode. J Mater Sci 43:3364–3369. doi:10.1007/s10853-008-2586-1